# Structural and functional analyses of Rubisco from arctic diatom species reveal unusual posttranslational modifications

Karin Valegård[‡], P. John Andralojc[§1], Richard P. Haslam[§], F. Grant Pearce[‡2], Gunilla K. Eriksen[¶], Pippa J. Madgwick[§1], Anne K. Kristoffersen[‖3], Michiel van Lun[‡], Uwe Klein[‖], Hans C. Eilertsen[¶], Martin A. J. Parry[§1,4], and Inger Andersson[‡5]

From the [‡]Department of Cell and Molecular Biology, Uppsala University, Box 596, S-751 24 Uppsala, Sweden, [§]Department of Plant Science, Rothamsted Research, Harpenden, Herts AL5 2JQ, United Kingdom, the [¶]Norwegian College of Fisheries Science, Arctic University of Norway, N-9037 Tromsø, Norway, and the [‖]Department of Biosciences, University of Oslo, P.O. Box 1066, Blindern, N-0316 Oslo, Norway

Edited by Ruma Banerjee

The catalytic performance of the major $CO_2$-assimilating enzyme, ribulose-1,5-bisphosphate carboxylase/oxygenase (Rubisco), restricts photosynthetic productivity. Natural diversity in the catalytic properties of Rubisco indicates possibilities for improvement. Oceanic phytoplankton contain some of the most efficient Rubisco enzymes, and diatoms in particular are responsible for a significant proportion of total marine primary production as well as being a major source of $CO_2$ sequestration in polar cold waters. Until now, the biochemical properties and three-dimensional structures of Rubisco from diatoms were unknown. Here, diatoms from arctic waters were collected, cultivated, and analyzed for their $CO_2$-fixing capability. We characterized the kinetic properties of five and determined the crystal structures of four Rubiscos selected for their high $CO_2$-fixing efficiency. The DNA sequences of the *rbc*L and *rbc*S genes of the selected diatoms were similar, reflecting their close phylogenetic relationship. The $V_{max}$ and $K_m$ for the oxygenase and carboxylase activities at 25 °C and the specificity factors ($S_{c/o}$) at 15, 25, and 35 °C were determined. The $S_{c/o}$ values were high, approaching those of mono- and dicot plants, thus exhibiting good selectivity for $CO_2$ relative to $O_2$. Structurally, diatom Rubiscos belong to form I C/D, containing small subunits characterized by a short $\beta A$–$\beta B$ loop and a C-terminal extension that forms a $\beta$-hairpin structure ($\beta E$–$\beta F$ loop). Of note, the diatom Rubiscos featured a number of posttranslational modifications of the large subunit, including 4-hydroxyproline, $\beta$-hydroxyleucine, hydroxylated and nitrosylated cysteine, mono- and dihydroxylated lysine, and trimethylated lysine. Our studies suggest adaptation toward achieving efficient $CO_2$ fixation in arctic diatom Rubiscos.

Ribulose-1,5-bisphosphate carboxylase/oxygenase (Rubisco[6]; EC 4.1.1.39) is the principal enzyme responsible for the assimilation of $CO_2$ into the biosphere. It catalyzes the primary photosynthetic $CO_2$ reduction reaction, the carboxylation of D-ribulose 1,5-bisphosphate (RuBP) by $CO_2$. The product of this reaction, 3-phosphoglycerate (3PGA), is subsequently converted into biomass. Rubisco is found in all photoautotrophic organisms, including photosynthetic bacteria, archaea, algae, and plants. The oceans are of particular importance for the global carbon cycle and are estimated to have a net uptake flux of about 2 petagrams (Pg) of carbon/year (1). This takes place as pressure difference–driven diffusion influenced by wind and enhanced by sequestration by marine phytoplankton. Oceanic contribution to the global net primary production (NPP) has been estimated to 45–50 Pg of carbon/year (2), which amounts to about 45% of the total NPP. This is remarkable, considering the low availability of free dissolved $CO_2$ and its slow diffusion in sea water, but is connected to the overall fast growth rates of phytoplankton, often leading to a $\gg$50% increase in biomass per day (3).

Carbon fixation resulting from Rubisco's activity amounts to more than $10^{11}$ tons of atmospheric $CO_2$ annually (2). However, Rubisco is an inefficient catalyst because of its low turnover rate and its tendency to catalyze a reaction with $O_2$ rather than $CO_2$, leading to the oxygenation of its sugar phosphate substrate to yield 2-phosphoglycolate (2PG). This inherent oxy-

[6] The abbreviations used are: Rubisco, ribulose-1,5-bisphosphate carboxylase/oxygenase; RuBP, D-ribulose 1,5-bisphosphate; 3PGA, 3-phospho-D-glycerate; Pg, petagrams; 2PG, 2-phosphoglycolate; NPP, net primary production; L, large; S, small; *rbc*L, Rubisco large subunit gene; *rbc*S, Rubisco small subunit gene; CABP, 2′-carboxyarabinitol-1,5-bisphosphate; CCM, carbon-concentrating mechanism; Chla, chlorophyll *a*; Bicine, *N,N*-bis(2-hydroxyethyl)glycine; $\epsilon$-ACA, $\epsilon$-amino-*n*-caproic acid.

genase activity leads to a significant loss of carbon to the atmosphere and a decrease in the carboxylation efficiency (for reviews, see, for example, Refs. 4–6). Because of the significance of Rubisco to crop production, plant nitrogen and water usage, and the global carbon cycle, there is considerable interest in investigations aimed at reducing the oxygenase activity. Rubisco has been the subject of intense research, including structural, mechanistic, and mutagenesis studies. However, despite the vast amount of data available, the molecular basis for its $CO_2/O_2$ discrimination is not fully understood.

The ratio of carboxylation and oxygenation, measured as the $CO_2/O_2$ specificity factor (for a definition, see below), is not fixed, and there is substantial variation among phototrophs (7). For instance, the specificity factor is very low (around 20) in anoxygenic nonsulfur purple bacteria but considerably higher (∼80–100) in Rubisco from green plants. Form I Rubisco, to which plant Rubiscos belong, can be further divided into two subgroups: green-like, containing higher plants, green algae, and cyanobacteria, and red-like, containing among others eukaryotic nongreen algae (*i.e.* diatoms and rhodophytes) (8–10). The latter group contain some of the most $CO_2$-efficient forms of Rubisco.

The genetic, phylogenetic, kinetic, and structural characteristics of red-like Rubiscos from marine organisms are to a large extent unknown. For example, little is known about Rubisco from psychrophilic organisms that live in arctic waters. The objective of the present work was therefore to study arctic/cold water microalgae to provide new information on Rubisco function at the molecular level. We have studied the natural variation in Rubisco from northern diatoms, which thrive at the light-limited low temperature environments within and below the ice and make up the main part of primary production in fish-rich areas (11).

## Results

### Growth experiments

The growth data were standardized to compare measurements obtained by different methods (see "Experimental procedures") and hence only serve the purpose of comparing the species in a relative manner. The mean growth rate obtained from the different methods was 0.47 doublings/day, with a minimum of ∼0.05 and maximum of ∼1.2 doublings/day. The expected maximum doubling rate at 3–4 °C is ∼1.0 doublings/day (12); considering that we used a light/dark photoperiod of 14 h/10 h, we conclude that the growth achieved for our seven chosen species was in the maximum range. The results from the growth rate experiments showed that the overall fastest grower at 2–3 °C was *Thalassiosira antarctica* (interpreted from the average growth data). In this temperature range, it was followed by *Bacterosira bathyomphala* and *Thalassiosira nordenskioeldii* (Table 1). The slowest growers in this temperature range were *Thalassiosira gravida* and *Thalassiosira hyalina*. At 7 °C, the fastest growers were *T. antarctica*, *B. bathyomphala*, and *T. nordenskioeldii*. When both temperatures were considered, the fastest growers were *T. antarctica*, *B. bathyomphala*, and *Chaetoceros socialis*; thus, *T. antarctica* performed best at both temperatures. The overall mean increase in growth rates from

**Table 1**

**Overall standardized maximum growth rates of seven diatom species chosen for further analysis**

The results are means of repeated experiments with species-specific $n > 48$. See "Experimental procedures" for explanation of the standardization method.

| Species | Maximum growth at 2–3 °C | Maximum growth at 7 °C |
|---|---|---|
| *C. socialis* | −0.19 | 0.09 |
| *T. nordenskioeldii* | 0.02[a] | 0.11 |
| *T. hyalina* | −0.24 | −0.32[a] |
| *T. antarctica* | 0.54[a] | 0.12 |
| *T. gravida* | −0.25 | −0.08 |
| *S. marinoi* | −0.22 | −0.11[a] |
| *B. bathyomphala* | 0.13[a] | 0.12[a] |

[a] Species that had standardized growth rates statistically significantly different from the other species at the same temperature (analysis of variance, $p < 0.05$).

low to high temperature regimes were ∼0.03 (in standardized relative units), and only *C. socialis*, *T. nordenskioeldii*, *T. gravida*, and *Skeletonema marinoi* responded with increased growth rates when the temperature increased (Table 1).

### Determination of kinetic constants of Rubisco enzymes from arctic diatoms

The $CO_2$-fixation efficiency of Rubisco shows considerable species-specific variation (13). Our objective was to identify the most efficient Rubiscos among diatoms, a group of microalgae that are prime candidates for finding new highly efficient Rubisco enzymes. The partitioning between the carboxylation and oxygenation reactions ($v_c/v_o$) depends on the relative concentrations of the gaseous substrates and the relative catalytic efficiencies ($V_{max}/K_m$) of the two activities in accordance with the relationship, $v_c/v_o = (V_c K_o/V_o K_c)$ ([$CO_2$]/[$O_2$]), where $v_c$ and $v_o$ are the velocities of carboxylation and oxygenation, respectively, $V_c$ and $V_o$ are the maximal velocities of the two reactions, and $K_c$ and $K_o$ are the Michaelis constants for $CO_2$ and $O_2$, respectively. The composite of constants in the equation is referred to as the specificity factor and is often referred to as $S_{c/o}$, $\tau$, or $\Omega$ (14). The specificity factor is usually determined from the product of the measured 3PGA/2PG concentrations and the known [$CO_2$]/[$O_2$] ratio.

Optimization of a Rubisco purification procedure for use with marine diatoms was undertaken, and a suitable protocol was developed that resulted in over 80% pure Rubisco. Diatom Rubisco content was generally much lower than in plants, confirming earlier observations (15).

HPLC analysis of [$^{14}$C]RuBP oxygenation and carboxylation was first evaluated to examine diatom Rubisco $CO_2/O_2$ specificity. This method is labor-intensive, highly sensitive to relatively small changes in 3PGA and 2PG concentrations, and requires tightly controlled reaction conditions. Therefore, a method based on the oxygen electrode was employed, giving real-time data collection. Wheat Rubisco was used as an internal standard. In addition, $K_m$ and $V_{max}$ were determined for Rubisco from diatom species with wheat as a control.

Using assays and screening protocols especially developed for diatom Rubisco enzymes, specificity factors were determined for five diatom species at a range of temperatures from 15 to 35 °C (Table 2) (16). The specificity factors of diatom Rubiscos were close to that for wheat Rubisco. In all of the arctic

**Table 2**
Relative specificities and kinetic constants of Rubisco from marine diatoms

| Species | Temperature | Normalized specificity factors | | | Kinetic constants ($n = 6$) | | | |
|---|---|---|---|---|---|---|---|---|
| | | Mean | S.D. | $n$ | $V_c$max | $V_o$max | $K_m$C | $K_m$O |
| | *°C* | | | | *µmol min$^{-1}$ mg Rubisco$^{-1}$* | *µmol min$^{-1}$ mg Rubisco$^{-1}$* | *µM* | *mM* |
| *T. hyalina* | 15 | 106 | 4 | 4 | | | | |
| | 25 | 99 | 3 | 4 | 3.5 ± 0.1 | 1.2 ± 0.2 | 50 ± 3 | 1.64 ± 0.20 |
| | 35 | 87 | 1 | 3 | | | | |
| *B. bathyomphala* | 15 | 94 | 10 | 3 | | | | |
| | 25 | 87 | 4 | 3 | 3.9 ± 0.1 | 0.8 ± 0.1 | 81 ± 4 | 1.30 ± 0.18 |
| | 35 | 76 | 2 | 3 | | | | |
| *S. marinoi* | 15 | 96 | 9 | 4 | | | | |
| | 25 | 96 | 7 | 4 | 4.0 ± 0.1 | 1.6 ± 0.2 | 48 ± 2 | 1.81 ± 0.19 |
| | 35 | 84 | 5 | 3 | | | | |
| *T. nordenskioeldii* | 25 | 82 | 2 | 5 | 4.0 ± 0.1 | 0.6 ± 0.1 | 122 ± 4 | 1.42 ± 0.53 |
| *T. antarctica* | 25 | 90[a] | 3.2[a] | 5[a] | 3.2 ± 0.2 | 0.7 ± 0.3 | 93 ± 10 | 1.74 ± 0.75 |
| *T. aestivum* | 15 | 113 | 8 | 4 | | | | |
| | 25 | 100 | 3 | 4 | 2.5 ± 0.1[b] | 0.8 ± 0.03[b] | 10.9 ± 0.9[b] | 0.34 ± 0.03[b] |
| | 35 | 90 | 3 | 3 | | | | |

[a] From Ref. 16.
[b] From Ref. 57.

species examined, the specificity factor increased at decreasing temperatures. None of the arctic species examined had a higher specificity factor than wheat, even when values were extrapolated to 0 °C. However, unlike wheat Rubisco, diatom Rubiscos were not deactivated when exposed for prolonged periods (~24 h) to temperatures of 4 °C (data not shown). These observations suggest structural adaptations to the low temperatures in the extreme environment these diatoms occupy.

### Crystal structures of Rubisco enzymes from arctic diatoms

Crystals of diatom Rubisco species were obtained, and the corresponding structures were determined. Details of data collection and refinement are summarized in Table 3. Overall, the quality and resolution of the data were very good, with the best crystals diffracting to better than 2 Å resolution. However, because some crystals were thin in at least one dimension, the corresponding data were anisotropic. The quality of the structures was significantly improved by the use of TLS refinement implemented in the refinement programs REFMAC5 and PHENIX, but the quality of the *T. nordenskioeldii* and *B. bathyomphala* structures remained substandard, and they were not included in the final set of structures. The RbcL sequence from *T. nordenskioeldii* (O98947) was used for an initial fit to the electron density maps and subsequently modified to fit the density as refinement progressed. In parallel to this, genomic DNA was extracted from the cell cultures, and partial sequences of *rbc*L and *rbc*S were determined to aid model building (Fig. S1). The sequences of Rubisco from diatoms in this study were highly similar, as would be expected in view of their close relationship. GUG is the translation start codon of all *rbc*S genes sequenced. This codon normally codes for valine, but the protein structures show that, as expected, methionine was inserted in this position.

Diatom Rubisco (Fig. 1*A*) is a hexadecamer of eight large (L, 490 residues) and eight small (S, 139 residues) subunits and belongs to form I C/D (reviewed in Ref. 5). This form includes a small subunit that is distinct from the small subunits of form I A/B enzymes (*e.g.* in cyanobacteria and higher plants) and is

characterized by a short βA–βB loop and a C-terminal extension (βE–βF loop) that forms a β-hairpin structure. The β hairpins from four small subunits together form a β barrel that lines the entrance to the central solvent channel at each end of the holoenzyme (Fig. 1*B*). Form I C/D structures have previously been observed in Rubisco from the betaproteobacterium *Cupriavidus necator* (formerly *Ralstonia eutropha*), and the red algae *Galdieria partita* and *Galdieria sulfuraria* (17–19). The diatom structures are highly similar; structures can be superimposed with root mean square deviations of 0.15–0.32 Å for all Cα atoms.

### Posttranslational modifications

The structures of diatom Rubisco feature a number of posttranslational modifications in the large subunit (Table 4 and Figs. 2 and 3). Rubisco is activated by carbamoylation of the ε-amino group of an active-site lysine residue and subsequent coordination to $Mg^{2+}$ (20, 21). Thus, as expected for the fully activated enzyme examined in the present study, electron density corresponding to a carbamoyl group is observed at the ε-amino group of Lys-205 (corresponding to Lys-201 of spinach Rubisco). 4-Hydroxy-Pro residues are present at positions 48 and 155. Hydroxy-Pro-155 (Fig. 2*A*) corresponds to hydroxy-Pro-151 of Rubisco from the green algae *Chlamydomonas reinhardtii* (22), whereas hydroxy-Pro-48 appears to be unique to diatom Rubiscos. Both residues are relatively buried in the interior of the protein. Electron density corresponding to a modification of the sulfur atom of Cys-109 was detected in some (*T. antarctica*, *T. hyalina*, *B. bacterosira*) but not all diatoms. Analysis of this extra density shows that it is most consistent with hydroxylation. A large extra density at Sγ of Cys-457 suggested a different modification; we first considered carbamylation or methylation (methylcysteine was detected in Rubisco from *C. reinhardtii* (22)), but analysis of side-chain atom temperature factors and difference density maps after refinement indicated such modifications to be unlikely. Instead, nitrosylation of the Cys-sulfur was found to best fit the extra density (Fig. 2*B*). The *S*-nitroso group of Cys-457 is accessible to solvent,

**Table 3**
**Data collection and refinement statistics**
Values in parentheses are for the outer-resolution shell.

| | *T. antarctica* var. borealis | *T. hyalina* | *S. marinoi* | *C. socialis* |
|---|---|---|---|---|
| **PDB code** | 5MZ2 | 5N9Z | 6FTL | 5OYA |
| **Data collection** | | | | |
| X-ray source | ESRF ID14:2 | ESRF ID14:3 | Lund X711 | ESRF ID29 |
| Wavelength (Å) | 0.933 | 0.931 | 1.087 | 0.969 |
| Resolution (Å) | 1.9 | 1.9 | 2.6 | 1.8 |
| Space group | $P2_1$ | $P2_1$ | $P4_12_12$ | $C2$ |
| Unit cell parameters | | | | |
| $a, b, c$ (Å) | 118.3, 220.1, 124.4 | 118.0, 220.0, 124.3 | $a = b = 111.0, c = 396.4$ | 118.2, 219.1, 220.2 |
| $\beta$ (degrees) | 118.4 | 118.3 | | 90.2 |
| No. of reflections | 3,067,613 | 2,653,566 | 1,535,835 | 1,195,289 |
| No. of unique reflections | 437,345 | 432,731 | 75,003 | 495,177 |
| Completeness (%) | 99.9 (99.7) | 99.0 (98.5) | 96.9 (75.8) | 96.1 (94.9) |
| $R_{\text{merge}}$[a] | 0.117 (0.388) | 0.066 (0.251) | 0.178 (0.956) | 0.092 (0.668) |
| **Refinement** | | | | |
| Residues in model | L: 3/4-483/484 | L: 4-484 | L: 3-484 | L: 15/16-483 |
| | S: 1-139 | S: 1-139 | S: 1-139 | S: 1-139 |
| No water molecules | 3 659 | 3 107 | 354 | 2946 |
| No ethylene glycol molecules | 20 | 15 | 18 | 24 |
| $R_{\text{cryst}}$[b] | 0.143 (0.166) | 0.151 (0.179) | 0.171 (0.296) | 0.167 (0.317) |
| $R_{\text{free}}$[c] | 0.176 (0.218) | 0.182 (0.223) | 0.238 (0.364) | 0.192 (0.331) |
| r.m.s.d.[d] from ideal values | | | | |
| Bond lengths (Å) | 0.006 | 0.007 | 0.011 | 0.012 |
| Bond angles (degrees) | 0.922 | 0.973 | 1.57 | 1.36 |
| Ramachandran analysis (%) | | | | |
| Favored | 98 | 98 | 96 | 97 |
| Allowed | 2 | 2 | 4 | 3 |
| Outliers | 0 | 0 | 0 | 0 |

[a] $R_{\text{merge}} = \Sigma_{hkl} \Sigma_i |I_i(hkl) - \langle I(hkl)\rangle|/\Sigma_{hkl} \Sigma_i I_i(hkl)$, where $\langle I(hkl)\rangle$ is the average intensity of symmetry-equivalent reflections.
[b] $R_{\text{work}} = \Sigma_{hkl}||F_o| - |F_c||/\Sigma_{hkl}|F_o|$, where $F_o$ and $F_c$ are the observed and calculated structure factor amplitudes, respectively.
[c] $R_{\text{free}}$ calculated from a randomly chosen 5% of all unique reflections.
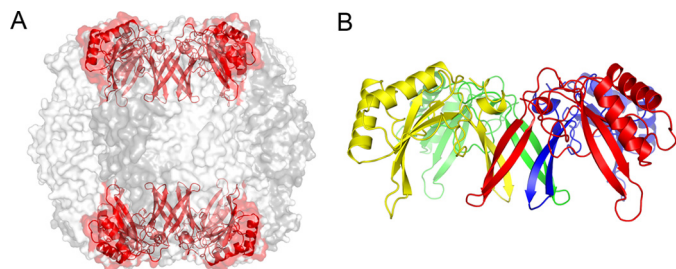[d] Root mean square deviation.

**Figure 1. Structure of form I D diatom Rubisco.** *A*, overall structure, showing large subunits in *two shades* of *gray* and small subunits in *red*. *B*, structure of the capping cluster of S subunits, *colored yellow*, *red*, *blue*, and *green*, respectively. The C-terminal strands from four different S subunits form a $\beta$-barrel that lines the central solvent channel.

suggesting that it may be involved in interactions with binding partners. Nitrosylation at Cys-457 was most prominent in Rubisco from *C. socialis*, but the modification could also be detected at lower occupancy in the enzymes from *T. antarctica* and *T. hyalina* (Table 4). It was only faintly detected in the enzyme from *S. marinoi*; this is probably because of the low resolution of the data. Lys-150 features additional density at C$\gamma$ and C$\delta$ most consistent with hydroxylation (Fig. 3). This is a relatively unusual modification that has not been reported previously. Lys-150 is located on the dimer interface of the large subunits and forms several hydrogen bonds with its 3- and 4-hydroxyl groups to Ser-147 of the adjacent subunit (Fig. 3*B*). Such contacts have been shown to influence stability, catalysis, and specificity in Rubisco (23–25). It is therefore likely that these interactions, which would not be present in the unmodified enzyme, will confer extra stability to the holoenzyme. Additional density at C$\delta$ of Lys-198 was interpreted as monohydroxylated lysine. Lys-346 shows extra density at its N$\epsilon$ cor-

responding to trimethylation (Fig. 2*C*). Trimethyl-Lys-346 is located at the exterior of the hexadecamer and is accessible to the solvent. Trimethyl-lysine has been detected at position 14 of some plants (26), although it has not yet been observed in a crystal structure, presumably due to disorder of the N terminus. Trimethylation of residue 346 appears to be unique to the present structures. Leu-174 is hydroxylated at C$\beta$ (Fig. 2*D*); the modification introduces an additional hydrogen bond contact to the main-chain nitrogen of Asp-202. As mentioned above, *rbc*S sequences deduced from the crystal structure differ from the DNA sequence at residue 1. All of the modifications are unambiguous for each of the 4–8 copies in the asymmetric unit.

## Discussion

Finding a Rubisco enzyme that has its carboxylation reaction enhanced relative to its oxygenase reaction and engineering this trait into the Rubisco enzymes of economically important crop plants has potential implications with regard to both agricultural and environmental considerations. Besides increasing yield, it would potentially allow the growth of crop plants in areas with a short season (*i.e.* short summers) and, in areas with longer seasons, permit more than one harvest per season. Current concerns regarding global warming and the greenhouse effect point to the need for a better understanding of global carbon fluxes, in particular in the oceans and between the ocean and the atmosphere.

Little is known about the biochemical properties of Rubisco from marine microorganisms, which are estimated to be responsible for about half of the total NPP. Initial findings indicate that Rubisco enzymes from marine microalgae carry a

**Table 4**
**Posttranslational modifications in diatom Rubiscos**

HYP, 4-hydroxyproline; CSO, *S*-hydroxycysteine; LYO, 4-hydroxylysine; LOH, 3,4-dihydroxylysine; 8RE, 3,4-dihydroxylysine; HLU, $\beta$-hydroxyleucine; HL2, $\beta$-hydroxyleucine; KCX, lysine-NZ-carboxylic acid; M3L, *N*-trimethyllysine; SNC, *S*-nitrosocysteine. LOH and 8RE are stereoisomers at the Cß position of dihydroxylysine. HLU and HL2 are stereoisomers at the Cß position of $\beta$-hydroxyleucine.

| Species | Pro-48 | Cys-109 | Lys-150 | Pro-155 | Leu-174 | Lys-198 | Lys-205 | Lys-346 | Lys-457 |
|---|---|---|---|---|---|---|---|---|---|
| *T. antarctica* | HYP | CSO | LYO | HYP | HLU | LYO | KCX | M3L | NM[a] |
| *T. hyalina* | HYP | CSO | 8RE | HYP | HLU | LYO | KCX | M3L | NM |
| *S. marinoi* | | NM | LOH | HYP | HLU | LYO | KCX | M3L | NM |
| *C. socialis* | HYP | CSO | LOH | HYP | HL2 | | KCX | M3L | SNC |

[a] NM, not modeled because of low occupancy.

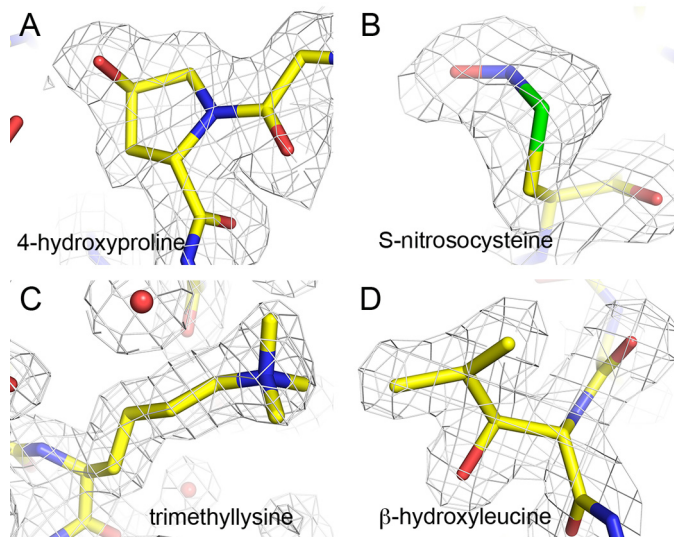**Figure 2. Representative electron density for posttranslationally modified residues.** *A*, 4-hydroxyproline. *B*, *S*-nitrosocysteine. *C*, $\epsilon$-N,N,N-trimethyllysine. *D*, $\beta$-hydroxyleucine.

number of unusual features that make them prime candidates for further studies. Young *et al.* (27) reported the kinetic constants of Rubisco enzymes from a set of diatoms, which were all of southern origin and had a relatively large geographic spread. Much less has been reported about the properties of Rubisco from northern diatoms, and no structures of diatom Rubisco have been described so far.

Specificity factors measured from diatom Rubisco are high relative to those of cyanobacteria. Although the specificity factor serves as an important first diagnostic parameter to indicate changes in efficiency of engineered Rubisco enzymes, it is but one parameter that determines the net efficiency of Rubisco enzymes. It is becoming increasingly obvious that environmental factors, such as the temperature and the aridity of the environment from which the organism evolved are important factors that influence Rubisco's carboxylation capacity (28). In the case of marine phytoplankton, $CO_2$ and light limitations are important factors to consider. Phytoplankton have adopted carbon-concentrating mechanisms (CCMs) to offset the problems of $CO_2$ limitation and use the high levels of bicarbonate in sea water (29, 30). Evidence for a CCM in diatoms to date is mainly from model diatoms (31), whereas direct evidence for a CCM in northern diatoms is currently lacking. Common with previously analyzed red-type Rubisco enzymes, the northern diatoms show a reduced affinity for $O_2$ (Table 2) but lack the very high affinity for $CO_2$ observed for nongreen algae, such as *Griffithsia monilis* (32, 33). This, together with the low concen-

tration of free dissolved $CO_2$ in sea water, would point to the need for a CCM. The operation of a CCM may increase photosynthetic light requirements. Thus, it seems possible that the evolution of high-specificity factors in diatoms (compared with, for example, ocean-living cyanobacteria) may contribute to their ability to grow well in the light-limited environment typical of the early bloom or under the arctic ice or during periods when the maximum solar elevation is low for longer periods (34). As the catalytic efficiency of Rubisco increases, one would expect that less nitrogen (as the constituent amino acids of Rubisco) would be required to maintain a given photosynthetic rate. From our results, the species that had the highest specificity factor relative to the others, *T. hyalina*/*T. antarctica*, also had the highest overall growth rate and the highest growth rate at the lowest (2 °C) temperature. In addition, the diatom with the lowest specificities, *S. marinoi*, is considered a more southern species that does not normally enter the true arctic growth regime (11). This, in our opinion, indicates that high-specificity Rubisco may be a cold water/arctic evolutionary adaptation connected to competitive advantages. Hobson *et al.* (35) have reported high specific activities and low cellular concentrations of Rubisco in diatoms relative to green algae, illustrating the coupling between carbon assimilation and nitrogen metabolism. Although speculative, improvements in Rubisco specificity would be ecologically significant if they affect the competitive ability of a species.

The Rubisco *rbc*L/S sequences obtained from genomic DNA extracted from the cultured diatom material were generally confirmed by the amino acid sequences deduced from the electron density maps. Most of the differences may not be of significant consequence for the function of the enzyme; for instance, the commonly observed Ile/Val substitution (or Ile/Leu) belongs to the same class of apolar amino acids with similar physico-chemical properties.

*T. nordenskioeldii*, *T. gravida*, and *T. antarctica* are common in the northern cold water to temperate regions (11), whereas *T. hyalina* is described as an arctic species (36). It is well known that it is difficult to distinguish morphologically between *Thalassiosira* species (*e.g.* the morphologically determined identity of *T. gravida* may be confused by the fact that it may change morphology when the temperature is lowered, whereby it resembles *T. rotula*) (37). *T. gravida* may also easily be misidentified with *T. antarctica* (38). There are also different "types" of *T. antarctica*; the one cultivated here probably most resembles *T. antarctica* var. borealis (39). In addition, the genetic information for the group is largely incomplete, and, as a consequence, the available species concepts may be incomplete, and phenotypic (and physiological) adaptation may well
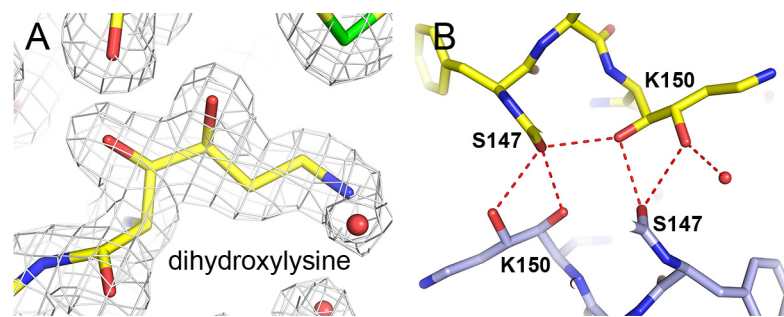
**Figure 3. Posttranslationally modified Lys-150.** *A*, electron density for $\gamma,\delta$-dihydroxylysine. *B*, contacts of the modified residue at the $L_2$ dimer interface. One L subunit is shown in *yellow* and the second L subunit in *blue*.

occur over short intervals of time. Considering the more southern origin of the diatoms that have been studied to date, the differences that we observe in this study may well be due to true variation occurring in the species collected in arctic/North Atlantic waters.

There is also the possibility that certain species may carry several copies of *rbc*L and/or *rbc*S genes and that these may be expressed differentially. Plants and green algae are known to have multiple nucleus-encoded *rbc*S genes; for instance, wheat carries over 20 *rbc*S genes, whereas *C. reinhardtii* has two copies (reviewed in Ref. 40). Some prokaryotes even have multiple copies of both *rbc*S and *rbc*L genes (41). Multiple copies are assumed to be the result of lateral gene transfer (8), but this has not been addressed specifically for diatoms. In addition, some chloroplasts have been found to exhibit maternal, paternal, and biparental modes of inheritance even within the same species; the latter has been shown in, for example, *Pseudo-nitzschia* (42). Whereas it is presently not possible to distinguish between these alternatives, it is not unlikely that the conditions in a mass culture may give rise to sequence variations (multiple sequences) in a manner observed here.

Whereas the carbamylation of an active-site lysine residue has been established as essential for activity, the roles of other posttranslational modifications of Rubisco have not been elucidated with regard to functional significance (reviewed in Refs. 43 and 44). Hydroxyproline is a major component of collagen, where the absence of the hydroxyl group on proline (caused by a deficiency in vitamin C) results in the disease scurvy. Hydroxyproline is also found in diverse proteins localized to the plant cell wall (45, 46), but this residue has never been observed in Rubisco from vascular plants. Whereas *S*-hydroxycysteine was detected here for the first time in Rubisco, 4-hydroxyproline and *S*-methylcysteine have been observed earlier in Rubisco from the unicellular green alga *C. reinhardtii* (22), but there is yet no known function for these modifications in algae. Redox regulation of Rubisco activity via cysteine residues has been extensively studied in *C. reinhardtii* (47). Nitric oxide (NO) signaling regulates various physiological processes in animals, plants, and algae. In the diatom *Skeletonema costatum*, a link has been found between nitric oxide concentrations and programmed cell death (48), suggesting a role for nitric oxide in the massive cell loss occurring at the end of a diatom bloom. Whether nitrosylation of Rubisco at Cys-457 is part of this mechanism remains to be elucidated, but we note that *S*-ni-

trosocysteine has also been detected at the corresponding position (Cys-460) in Rubisco from the red algae *G. sulfuraria* (19). The presence of mono- or dihydroxylated or trimethylated lysines in the diatom Rubisco enzymes investigated in this study is also enigmatic. Hydroxylysines have been detected in the hydrolysates of peptides and proteins exposed to $HO^{\bullet}/O_2$, and subsequently treated with $NaBH_4$ (49), but such oxidizing conditions are difficult to imagine in the live diatom cell. Hydroxylysine is a component of collagen and has also been reported to become incorporated instead of lysine in the bacterial cell wall (50). The diatom cell is characterized by its silica-based cell wall. Silica-precipitating peptides from the diatom *Cylindrotheca fusiformis* have been shown to contain posttranslationally modified lysines (51) that are necessary for their silica-precipitating activity. These lysine residues are $\epsilon$-dimethylated, $\epsilon$-trimethylated, or $\delta$-hydroxylated or contain a combination of these modifications. It is not clear why lysine residues of diatom Rubiscos should be modified in the same way. It may be that Rubisco has evolved to utilize the enzymes responsible for these modifications and that these confer some sort of advantage (*e.g.* insensitivity to tryptic proteolysis (44, 52) or stability). Occurrence of these modifications in all of the diatoms used in this study confirms their close relationship. Trimethylation of Lys-14 of the large subunit of Rubisco occurs in some plants (*e.g.* those belonging to the Solanaceae or Cucurbitaceae families), but not all (26, 43). It is possible that the interaction with other proteins (*e.g.* chaperones or Rubisco activase) may be regulated by trimethylation, but at present, there is no experimental evidence to substantiate this assumption. Similar to the *S*-nitroso-group of Cys-457, the trimethyl group of Lys-346 is located on the surface of the protein, thereby enabling potential contacts with other binding partners.

## Conclusion

Oceanic primary production is dominated by phytoplankton, and diatoms account for a significant proportion of the NPP (2, 3). Here, we present structural and functional data on a large set of diatoms from arctic cold waters. Our results indicate adaptation of diatom Rubiscos in response to the environment in which they live, including low contents of Rubisco protein, high specificity factors approaching those of the most efficient crop plants coupled with low oxygen sensitivities, and a number of posttranslational modifications.

## Experimental procedures

### Collection of algae in the arctic east ice area and selection of species for cultivation

To establish diatom monocultures, samples of algae were collected with 20-$\mu$m phytoplankton nets during three spring cruises to the Atlantic and arctic Barents Sea from 2004 to 2006. As an initial guideline, when species were selected, it was assumed that the quantitatively most important species recorded during field investigations were the fastest and most successful growers (for the compilation of abundances, see Ref. 11). The chosen potential candidates were representatives from the genera *Chaetoceros*, *Thalassiosira*, *Bactero-sira*, and *Skeletonema*.

### Growth rate measurements

Small-scale cultivation experiments were performed aimed at assessing the fastest growers at nutrient-replete conditions (*i.e.* $CO_2$ and autoclaved natural sea water with added nitrogen, phosphorous, and silicate to *f*/10 concentrations). These experiments were performed in irradiance and temperature-controlled/logged rooms at two irradiances and temperatures (fluorescent daylight tubes, light/dark = 14/10 h, scalar irradiance 25 and 125 $\mu$mol quanta m$^{-2}$ s$^{-1}$, 2–3 and 7 °C) using 25- and 1500-ml nontoxic Erlenmeyer plastic flasks. Because monitoring growth from a single measure of biomass (*e.g.* chlorophyll *a* (Chl*a*), which may vary with species and light level) may not be sufficient to detect "true" increase in overall biomass, several methods were applied to detect the fastest growers. The methods were increase in (i) cell numbers (inverted microscope counting), (ii) organic bound carbon and nitrogen (Carlo Erba Elemental analyzer), and (iii) *in vitro* Chl*a* and pheophytin content (53). We computed growth as doublings/day from the formula,

$$\mu = (\text{Log}_2 C2 - \log_2 C1)/D \tag{Eq. 1}$$

where $\mu$ represents doublings/day, *C2* and *C1* are cell numbers, and *D* is the number of days.

In addition, $^{14}$C radioactive tracer photosynthesis (carbon assimilation) measurements were performed applying 5-$\mu$Ci aqueous sodium bicarbonate/100 ml of culture (for detailed method, see Ref. 54). The scalar irradiance exposure gradients were 330, 172, 102, 53, 13, and 0 $\mu$mol quanta m$^{-2}$ s$^{-1}$. Further, we calculated both the $\alpha$-slope photosynthesis curve (mg C (mg Chl*a*)$^{-1}$ h$^{-1}$ $\mu$mol quanta m$^{-2}$ s$^{-1}$) and $P_{max}$ — maximum photosynthesis (mg C (mg Chl*a*)$^{-1}$ h$^{-1}$). The above experiments were repeated several times to achieve robust data sets for statistical analysis ($n = 2,680$). In the end, data for the highest growth rates, maximum photosynthesis ($P_{max}$), and slope photosynthesis ($\alpha$) for each species, condition, and experiment were standardized using the formula,

$$x_{new} = x - \mu/\sigma \tag{Eq. 2}$$

where $x$ is measured growth rate, $\mu$ is population mean doubling, and $\sigma$ is population S.D. The standardized results were then pooled for each species, the results were ranked, and the following seven diatom species were considered fast growers and were chosen for further investigation: *B. bathyomphala*,

*T. antarctica*, *T. hyalina*, *T. nordenskioeldii*, *T. gravida*, *C. socialis*, and *S. marinoi*.

### Mass cultivation

The selected species were mass cultured in specially constructed 300-liter plexiglass cylinders in temperature and irradiance-controlled rooms. Cultivation took place at ~4 °C under a 14/10-h light/dark regime and at optimal ($I_{max}$) scalar irradiances determined during the small-scale $^{14}$C experiments. When the desired culture densities had been reached (150–500 $\mu$g of Chl*a* liter$^{-1}$), the cultures were harvested onto specially designed 20-$\mu$m mesh plankton net devices. The samples were stored at $-80$ °C before further analysis.

### Purification of Rubisco for determination of specificity factors

Twenty-five ml of extraction buffer (100 mM Bicine, pH 8.0, 6% PEG 4000, 5 mM DTT, 1 mM each of benzamidine, phenylmethylsulfonyl fluoride, $\epsilon$-amino-*n*-caproic acid ($\epsilon$-ACA), and EDTA, 1% (v/v) Tween 80, 0.2 mM EGTA, 0.5% (w/v) polyvinylpolypyrrolidone, 0.5% (v/v) protease inhibitor mixture (Sigma P5955), and 1% (w/v) washed sand) was ground to a frozen powder in liquid nitrogen ($N_2$). To this was added 20–40 ml of a harvested mass culture from above, and then the mixture was ground to a frozen powder. A further 175 ml of extraction buffer was added, 25–50 ml at a time, with frequent grinding until thawing was complete. On thawing, polysaccharide hydrolases were added (200,000 units of lysozyme, 40 units of pectinase, 8 units of cellulase, all supplied by Sigma UK), and the ice-cold homogenate was sonicated (6–8-$\mu$m amplitude) for 30 s followed by a 60-s interval. This was repeated until the total sonication time was 2 min. The extract was clarified by centrifugation (22,000 × *g*, 20 min, 4 °C), brought to 20% (w/v) PEG 4000 and 20 mM $MgCl_2$, and then stirred for 30 min at 4 °C. The resulting protein precipitate was sedimented by centrifugation (22,000 × *g*, 20 min, 4 °C) and redissolved in 8 ml of ice-cold gradient buffer (10 mM Tris, pH 8.0 (HCl), 10 mM $MgCl_2$, 10 mM $NaHCO_3$, 5 mM DTT, 1 mM EDTA, 1 mM $KH_2PO_4$, 1 mM benzamidine, 1 mM $\epsilon$-ACA), using a precooled homogenizer to achieve a lump-free suspension. The suspension was clarified by centrifugation (235,000 × *g*, 20 min, 4 °C), applied to a previously prepared sucrose gradient (0.3–1.2 M sucrose in gradient buffer) at a rate of 4 ml of suspension per 35 ml of sucrose gradient, centrifuged for 190 min at 370,000 × *g* at 4 °C, fractionated into 1-ml aliquots, and then snap-frozen in liquid $N_2$. A small sample previously taken from each fraction was assayed for protein content and Rubisco activity (55). Fractions containing the Rubisco activity peak (between fraction 9 and 14 from the bottom) were pooled and passed through PD-10 columns (2 ml of sample/column) pre-equilibrated in column buffer (100 mM Bicine, pH 8.1, 10 mM $MgCl_2$, 10 mM $NaHCO_3$, 5 mM DTT, 0.5 mM EDTA, 1 mM $\epsilon$-ACA, 1 mM benzamidine, 1 mM $KH_2PO_4$). The resulting protein eluates were combined and passed through 0.45-$\mu$m regenerated cellulose filters before sample concentration using Centriplus concentrators (Millipore Amicon, 150,000 NMWL). The final volume of the resulting Rubisco was ~0.50 ml, which was snap-frozen in liquid $N_2$ before short-term storage at $-80$ °C.

Preparation of Rubisco used for determination of kinetic constants used a simplified procedure, omitting the sonication, sucrose gradient, and ultrafiltration treatments, simply consisting of homogenization, sedimentation, PEG precipitation, clarification of the redissolved protein, and passage through PD-10 columns pre-equilibrated with column buffer supplemented with 2% (w/v) PEG 4000, followed by freezing in liquid $N_2$, before short-term storage at $-80$ °C.

### Determination of specificity factors

Specificity factors for diatom Rubisco were determined by real-time data collection based on rates of carboxylation and oxygenation measured by $^{14}$C incorporation and an oxygen electrode, respectively. Wheat Rubisco was used as an internal standard, and before use, a freeze-dried stock of wheat Rubisco was dissolved in $CO_2$-free 0.1 M Bicine, pH 8.2, containing 20 mM $MgCl_2$. The purified Rubisco samples were then desalted by centrifugation through G25 Sephadex columns previously equilibrated with $CO_2$-free 0.1 M Bicine, pH 8.2, containing 20 mM $MgCl_2$. Potassium phosphate (400 mM, pH 8.2) was then added to give a final concentration of 4 mM. NaH$^{14}$CO$_3$ (37 GBq mol$^{-1}$) was then added to a final concentration of 10 mM, and the wheat Rubisco was activated by incubation at 37 °C for 40 min. Diatom Rubisco showed no increase in activity in response to warming but maintained activity for 24 h when kept at 4 °C (data not shown). Reaction mixtures were prepared in an oxygen electrode (model DW1, Hansatech, Kings Lynn, UK) by first adding 0.95 ml of 100 mM Bicine, pH 8.1, containing 10 mM $MgCl_2$ and 20 $\mu$g (50 WA units) of carbonic anhydrase, pre-equilibrated with $CO_2$-free air at 25 °C, and 0.02 ml of 0.1 M NaH$^{14}$CO$_3$, 18.5 GBq/mol. A sufficient amount of activated Rubisco was then added in 25 $\mu$l to complete the reaction in 5 min. The reaction was started by the addition of 10 $\mu$l of 18.5 mM RuBP. RuBP oxygenation was calculated from the oxygen consumption and carboxylation from the amount of $^{14}$C incorporated into 3PGA when all of the RuBP was consumed (56). A number of reaction mixtures containing pure wheat Rubisco were interspersed with those containing Rubisco from diatoms. In addition, measurements of specificity at 15 and 35 °C were made. The procedure followed was similar to that at 25 °C. Mean initial concentrations of $O_2$ in solution in equilibrium with air were 305, 254, and 227 $\mu$M at 15, 25, and 35 °C, respectively, as determined by the integrated Hansatech software. Initial concentrations of $CO_2$ in solution were calculated from the amounts of NaHCO$_3$ added, using p$K_a$ values for $H_2CO_3$ of 6.19, 6.11, and 6.06 at 15, 25, and 35 °C, respectively. The specificity values were normalized to the average value for wheat Rubisco, of 94 $\pm$ 4 (S.D.) ($n = 4$) at 25 °C. The determinations were repeated 3–5 times at each temperature, using material pooled from two or three biological replicates.

### Determination of catalytic parameters

Catalytic parameters were measured essentially as described previously (57). Carboxylation activity was measured at 8, 16, 24, 36, 68, and 100 $\mu$M $CO_2$ (aqueous) in equilibrium with a gas phase of $N_2$ containing 2, 21, 56, or 92% (v/v) $O_2$ at 25 °C. $K_m$ and $V_{max}$ for carboxylation ($K_c$ and $V_c$, respectively) were cal-

culated at each $O_2$ concentration using a Michaelis–Menten kinetic model. $K_m$ and $V_{max}$ for oxygenation ($K_o$ and $V_o$, respectively) were calculated as follows: $K_o = [O_2]/((K_{m,app}/K_c) - 1)$ and $V_o = (V_c \times K_o)/(K_c \times S_{c/o})$, where $K_c$ is the $K_m$ for $CO_2$ in the absence of $O_2$, and $K_{m,app}$ is the apparent $K_m$ for $CO_2$, as measured in the reactions equilibrated with 21, 56, or 92% $O_2$. Specific mixtures of $N_2$ and $O_2$ were prepared using a gas divider (Signal Group, Camberley, UK), and concentrations of $O_2$ in solution were calculated at 100% relative humidity and standard atmospheric pressure (101.3 kilopascals). The solubility of $O_2$ was taken as 257.5 $\mu$M. The concentration of $CO_2$ in solution (in equilibrium with HCO$_3^-$) was calculated assuming a p$K_a$ of 6.11 for the first ionization of carbonic acid, taking into consideration the pH of each buffer solution (measured on the day of assay). Carbonic anhydrase ($\geq$50 WA units/1-ml reaction; Sigma, Poole, UK) was present in the reaction solution to maintain equilibrium between NaHCO$_3$ and $CO_2$. The Rubisco samples used in these assays had all been equilibrated in NaHCO$_3$- and $MgCl_2$-containing buffers during the purification procedures (above) and were found not to require any further activation before assay. Control reactions were performed by measuring $CO_2$ fixation (acid-stable $^{14}$C) in reaction solutions lacking RuBP or NaHCO$_3$ and following substitution of RuBP for 3PGA or following total inhibition of Rubisco by prior treatment with an excess of the tight-binding Rubisco inhibitor, 2′-carboxyarabinitol-1,5-bisphosphate (CABP). These controls confirmed that the activity measured (*i.e.* all acid-stable $^{14}$C detected) was entirely due to Rubisco.

Radioactive content of $^{14}$C-labeled compounds was measured in 0.40-ml aqueous solutions, following the addition of 3.6 ml of Ultima Gold scintillation mixture (PerkinElmer), using a Tri-Carb 2910 TR Liquid Scintillation Analyzer (PerkinElmer Life Sciences, Seer Green, UK).

Values of Michaelis–Menten constants and maximum velocities were estimated using EnzFitter (Biosoft, Cambridge, UK). Turnover number ($k_{cat}$; mol of product $\times$ mol of active site$^{-1}$ $\times$ s$^{-1}$) was calculated from the corresponding $V_{max}$ values ($V_c$ and $V_o$; $\mu$mol of product $\times$ mg of Rubisco$^{-1}$ $\times$ min$^{-1}$) after determination of Rubisco concentration in the samples. This was accomplished using the [$^{14}$C]CABP-binding assay described previously (58).

### Sequencing of Rubisco genes from marine diatom species

Total genomic DNA was isolated, and the DNAs were used as templates in PCRs to amplify the *rbc*L/S genes. Internal PCR primers were designed according to marine algal *rbc*L/S sequences that are already deposited in databases. Sequences of the 5′ and 3′ ends of the genes were amplified using the internal and a set of external primers designed according to genes flanking the *rbc*L/S gene cluster. These genes were found in a preliminary assembly of the genome of the diatom *T. pseudonana* on the website of the Joint Genome Institute of the United States Department of Energy (http://www.jgi.doe.gov/).

Genomic DNA from *C. socialis*, *T. antarctica*, *T. hyalina*, *T. nordenskioeldii*, *S. marinoi*, and *B. bathyomphala* was extracted by standard methods. Oligonucleotides were designed to amplify a region of the diatom genome including the Rubisco large and small subunit genes, *rbc*L and *rbc*S. In most cases, a faithful

DNA polymerase (PicoMaxx from Stratagene) was used to amplify this region, and the sequences of *rbc*L and *rbc*S from each species were determined. For each species, each base has been covered by at least two sequencing reactions from independently generated PCR products. If there was any difference between the first two sequences, a third independently generated PCR fragment was sequenced. Two species initially gave more than one DNA sequence. In these cases, sequencing was repeated with DNA isolated from a new culture.

### Isolation and purification of Rubisco for structure determination

To yield crystallization-grade purity, frozen algae in glycerol ($\sim$20 g) were thawed and suspended in 10 ml of extraction buffer (50 mM Bicine, pH 8.0, 10 mM MgCl$_2$, 10 mM NaHCO$_3$, 1 mM EDTA, 5 mM 2-mercaptoethanol, 1 Complete protease inhibitor tablet (Roche Molecular Biochemicals), 5 $\mu$l of Benzonase nuclease (Novagen)). The algal suspension was disrupted in a One-shot cell disrupter (Constant System Ltd.). The extract was centrifuged (15 min, 20,000 rpm, Sorvall SS34). The supernatant was passed through a 0.45-$\mu$m syringe filter and applied to a Superdex 200 column (120 ml) equilibrated with purification buffer. Fractions (2 ml) were collected and analyzed by SDS-PAGE. Fractions containing Rubisco were pooled, diluted with an equal volume of 0.1 M NaCl in purification buffer, and further purified on a MonoQ ion-exchange column (8 ml). The sample was loaded onto the column and equilibrated with low salt (0.1 M NaCl in purification buffer). The protein was eluted with a linear 0.1–0.5 M NaCl gradient in 120 ml of purification buffer. Fractions (2 ml) were collected and analyzed by SDS-PAGE. Pooled fractions containing Rubisco yielded 2–5 mg of pure protein from 20 g of algae.

### Crystallization, data collection, structure determination, and refinement

Before crystallization, the activated enzyme was concentrated to 20 mg ml$^{-1}$ using Vivaspin 6 (Vivascience) and incubated with 0.001 M CABP. Crystals were grown using the hanging-drop vapor diffusion method at 20 °C. The drop contained equal amounts of the protein sample in crystallization buffer (0.05 M HEPES, pH 7.5, 0.05 M NaCl, 0.01 M NaHCO$_3$, and 0.005 M MgCl$_2$) with 0.001 M CABP added, and a well solution consisting of the crystallization buffer with 7–13% PEG 4000 as a precipitating agent. The crystals were flash-cooled in liquid N$_2$ using a mother liquor with 30% ethylene glycol added as a cryoprotectant and maintained at 100 K for data collection. Diffraction data were collected at Max-lab (Lund, Sweden) and at the European Synchrotron Radiation Source (Grenoble, France) (Table 3). The data were processed using DENZO/SCALEPACK (59) and XDS (60). The crystal structures were solved by molecular replacement using the program MOLREP (61). The initial search model consisted of a set of one large and one small subunit of *G. partita* Rubisco (Protein Data Bank code 1BWV). Using the data for Rubisco from *T. antarctica*, eight solutions corresponding to eight different orientations of the search model in the hexadecamer of the asymmetric unit were found. The RbcL sequence from *T. nordenskioeldii* (O98947) was used for an initial fit to the electron density maps; this crude fit was subsequently improved using results obtained from sequencing of the gene and by inspection of electron density maps. Subsequently, the refined model of *T. antarctica* Rubisco was used as a search model to solve the remaining structures (Table 3). Modifications of the sequence were made as above.

Refinement was performed using REFMAC5 (62) and PHENIX (63). For cross-validation, 5% of the data were excluded from the refinement for $R_{\text{free}}$ calculations. Refinement consisted of one round of rigid-body refinement using data to 3 Å, followed by refinement using a maximum likelihood target function with noncrystallographic symmetry restraints. Noncrystallographic symmetry restraints were released toward the end of refinement of the structures to the highest resolution. TLS refinement (64) was used in the final stages with each subunit as a TLS group. Solvent molecules were added using ARP/wARP (65) and were manually inspected in O (66). Throughout the refinement, the $2mF_o - DF_c$ and $mF_o - DF_c$ $\sigma$A weighted maps (67) were inspected, and the models were manually adjusted using O (66).

## References

1. Takahashi, T., Sutherland, S. C., Sweeney, C., Poisson, A., Metzl, N., Tilbrook, B., Bates, N., Wanninkhof, R., Feely, R. A., Sabine, C., Olafsson, J., and Nojiri, Y. (2002) Global sea-air CO$_2$ flux based on climatological surface ocean pCO$_2$, and seasonal biological and temperature effects. *Deep Sea Res. Part 2 Top Stud. Oceanogr.* **49,** 1601–1622 CrossRef

2. Field, C. B., Behrenfeld, M. J., Randerson, J. T., and Falkowski, P. (1998) Primary production of the biosphere: Integrating terrestrial and oceanic components. *Science* **281,** 237–240 CrossRef Medline

3. Falkowski, P. (2012) Ocean science: the power of plankton. *Nature* **483,** S17–S20 CrossRef Medline

4. Parry, M. A. J., Andralojc, P. J., Mitchell, R. A. C., Madgwick, P. J., and Keys, A. J. (2003) Manipulation of Rubisco: the amount, activity, function and regulation. *J. Exp. Bot.* **54,** 1321–1333 CrossRef Medline

5. Andersson, I., and Backlund, A. (2008) Structure and function of Rubisco. *Plant Physiol. Biochem.* **46,** 275–291 CrossRef Medline

6. Carmo-Silva, E., Scales, J. C., Madgwick, P. J., and Parry, M. A. J. (2015) Optimizing Rubisco and its regulation for greater resource use efficiency. *Plant Cell Environ.* **38,** 1817–1832 CrossRef Medline

7. Jordan, D. B., and Ogren, W. L. (1981) Species variation in the specificity of ribulose bisphosphate carboxylase/oxygenase. *Nature* **291,** 513–515 CrossRef

8. Delwiche, C. F., and Palmer, J. D. (1996) Rampant horizontal transfer and duplication of rubisco genes in eubacteria and plastids. *Mol. Biol. Evol.* **13,** 873–882 CrossRef Medline

9. Tabita, F. R. (1999) Microbial ribulose-1,5-bisphosphate carboxylase/oxygenase: a different perspective. *Photosynth. Res.* **60,** 1–28 CrossRef

10. Watson, G. M. F., and Tabita, F. R. (1997) Microbial ribulose 1,5-bisphosphate carboxylase/oxygenase: a molecule for phylogenetic and enzymological investigation. *FEMS Microbiol. Lett.* **146,** 13–22 CrossRef Medline

11. Degerlund, M., and Eilertsen, H. C. (2009) Main species characteristics of phytoplankton spring blooms in NE Atlantic and arctic waters (68–80°N). *Estuaries Coasts* **33,** 242–269

12. Eppley, R. W. (1972) Temperature and phytoplankton growth in sea. *Fishery Bull.* **70,** 1063–1085

13. Galmés, J., Kapralov, M. V., Andralojc, P. J., Conesa, M. À., Keys, A. J., Parry, M. A. J., and Flexas, J. (2014) Expanding knowledge of the Rubisco kinetics variability in plant species: environmental and evolutionary trends. *Plant Cell Environ.* **37,** 1989–2001 CrossRef Medline

14. Laing, W. A., Ogren, W. L., and Hageman, R. H. (1974) Regulation of soybean net photosynthetic $CO_2$ fixation by the interaction of $CO_2$, $O_2$, and ribulose 1,5-diphosphate carboxylase. *Plant Physiol.* **54,** 678–685 CrossRef Medline

15. Losh, J. L., Young, J. N., and Morel, F. M. M. (2013) Rubisco is a small fraction of total protein in marine phytoplankton. *New Phytologist* **198,** 52–58 CrossRef Medline

16. Haslam, R. P., Keys, A. J., Andralojc, P. J., Madgwick, P. J., Andersson, I., Grimsrud, A., Eilertsen, H. C., and Parry, M. A. J. (2005) Specificity of diatom Rubisco. in *Plant Responses to Air Pollution and Global Change* (Omasa, K., Nouchi, I., and De Kok, L. J., eds) pp. 157–164, Springer-Verlag, Tokyo

17. Hansen, S., Vollan, V. B., Hough, E., and Andersen, K. (1999) The crystal structure of Rubisco from *Alcaligenes eutrophus* reveals a novel central eight-stranded $\beta$-barrel formed by $\beta$-strands from four subunits. *J. Mol. Biol.* **288,** 609–621 CrossRef Medline

18. Sugawara, H., Yamamoto, H., Shibata, N., Inoue, T., Okada, S., Miyake, C., Yokota, A., and Kai, Y. (1999) Crystal structure of carboxylase reaction-oriented ribulose-1,5-bisphosphate carboxylase/oxygenase from a thermophilic red alga, *Galdieria partita*, *J. Biol. Chem.* **274,** 15655–15661 CrossRef Medline

19. Stec, B. (2012) Structural mechanism of RuBisCO activation by carbamylation of the active site lysine. *Proc. Natl. Acad. Sci. U.S.A.* **109,** 18785–18790 CrossRef Medline

20. Lorimer, G. H., Badger, M. R., and Andrews, T. J. (1976) The activation of ribulose-1,5-bisphosphate carboxylase by carbon dioxide and magnesium ions: equilibria, kinetics, a suggested mechanism, and physiological implications. *Biochemistry* **15,** 529–536 CrossRef Medline

21. Lorimer, G. H., and Miziorko, H. M. (1980) Carbamate formation on the $\epsilon$-amino group of a lysyl residue as the basis for the activation of ribulosebisphosphate carboxylase by $CO_2$ and $Mg^{2+}$. *Biochemistry* **19,** 5321–5328 CrossRef Medline

22. Taylor, T. C., Backlund, A., Spreitzer, R. J., Bjorhall, K., and Andersson, I. (2001) First crystal structure of Rubisco from a green alga, *Chlamydomonas reinhardtii. J. Biol. Chem.* **276,** 48159–48164 CrossRef Medline

23. Chen, Z., Chastain, C. J., Al-Abed, S. R., Chollet, R., and Spreitzer, R. J. (1988) Reduced $CO_2/O_2$ specificity of ribulose-bisphosphate carboxylase/oxygenase in a temperature-sensitive mutant of *Chlamydomonas. Proc. Natl. Acad. Sci. U.S.A.* **85,** 4696–4699 CrossRef

24. Karkehabadi, S., Taylor, T. C., Spreitzer, R. J., and Andersson, I. (2005) Altered intersubunit interactions in crystal structures of catalytically compromised ribulosebisphosphate carboxylase/oxygenase. *Biochemistry* **44,** 113–120 CrossRef Medline

25. van Lun, M., van der Spoel, D., and Andersson, I. (2011) Subunit interface dynamics in hexadecameric Rubisco. *J. Mol. Biol.* **411,** 1083–1098 CrossRef Medline

26. Houtz, R. L., Poneleit, L., Jones, S. B., Royer, M., and Stults, J. T. (1992) Posttranslational modifications in the amino-terminal region of the large subunit of ribulose- 1,5-bisphosphate carboxylase/oxygenase from several plant species. *Plant Physiol.* **98,** 1170–1174 CrossRef Medline

27. Young, J. N., Heureux, A. M. C., Sharwood, R. E., Rickaby, R. E. M., Morel, F. M. M., and Whitney, S. M. (2016) Large variation in the Rubisco kinetics of diatoms reveals diversity among their carbon-concentration mechanisms. *J. Exp. Bot.* **67,** 3445–3456 CrossRef Medline

28. Galmés, J., Flexas, J., Keys, A. J., Cifre, J., Mitchell, R. A. C., Madgwick, P. J., Haslam, R. P., Medrano, H., and Parry, M. A. J. (2005), Rubisco specificity factor tends to be larger in plant species from drier habitats and in species with persistent leaves. *Plant Cell Environ.* **28,** 571–579 CrossRef

29. Giordano, M., Beardall, J., and Raven, J. A. (2005) $CO_2$ concentrating mechanisms in algae: mechanisms, environmental modulation, and evolution. *Annu. Rev. Plant Biol.* **56,** 99–131 CrossRef Medline

30. Reinfelder, J. R. (2010) Carbon concentrating mechanisms in eukaryotic marine phytoplankton. *Annu. Rev. Mar. Sci.* **3,** 291–315

31. Hopkinson, B. M., Dupont, C. L., and Matsuda, Y. (2016) The physiology and genetics of $CO_2$ concentrating mechanisms in model diatoms. *Curr. Opin. Plant Biol.* **31,** 51–57 CrossRef Medline

32. Badger, M. R., Andrews, T. J., Whitney, S. M., Ludwig, M., Yellowlees, D. C., Leggat, W., and Price, G. D. (1998) The diversity and coevolution of Rubisco, plastids, pyrenoids, and chloroplast-based $CO_2$-concentrating mechanisms in algae. *Can. J. Bot.* **76,** 1052–1071 CrossRef

33. Savir, Y., Noor, E., Milo, R., and Tlusty, T. (2010) Cross-species analyses traces adaption of Rubisco toward optimality in a low-dimensional landscape. *Proc. Natl. Acad. Sci. U.S.A.* **107,** 3475–3480 CrossRef Medline

34. Eilertsen, H. C., and Degerlund, M. (2010) Phytoplankton and light during the northern high-latitude winter. *J. Plankton Res.* **32,** 899–912 CrossRef

35. Hobson, L. A., Morris, W. J., and Guest, K. P. (1985) Varying photoperiod, ribulose 1,5-bisphosphate carboxylase/oxygenase and $CO_2$ uptake in *Thalassiosira fluviatilis* (Bacillariophyceae). *Plant Physiol.* **79,** 833–837 CrossRef Medline

36. Smayda, T. (1958) Biogeographical studies of marine phytoplankton. *Oikos* **9,** 158–191 CrossRef

37. Syvertsen, E. E. (1977) *Thalassiosira rotula* and *T. gravida*: ecology and morphology. *Nova Hedwigia* **54,** 99–112

38. Quillfeldt, C. H., von. (2001) Identification of some easily confused common diatom species in arctic spring blooms. *Botanica Marina* **44,** 375–389

39. Hasle, G. R., and Syvertsen, E. E. (1997) Marine diatoms. In *Identifying Marine Phytoplankton* (Thomas, C. R., Ed) pp. 5–385, Academic Press, Inc., San Diego

40. Spreitzer, R. J. (2003) Role of the Rubisco small subunit. *Arch. Biochem. Biophys.* **414,** 141–149 CrossRef Medline

41. Heinhorst, S., Baker, S. H., Johnson, D. R., Davies, P. S., Cannon, G. C., and Shively, J. M. (2002) Two copies of Form I RuBisCO genes in *Acidithiobacillus ferrooxidans* ATCC 23270. *Curr. Microbiol.* **45,** 115–117 CrossRef Medline

42. Levialdi Ghiron, J. H., Amato, A., Montresor, M., and Kooistra, W. H. C. F. (2008) Plastid inheritance in the planktonic raphid pennate diatom *Pseudo-nitzschia delicatissima* (Bacillariophyceae). *Protist* **159,** 91–98 CrossRef Medline

43. Houtz, R. L., and Portis, A. R. (2003) The life of ribulose 1,5-bisphosphate carboxylase/oxygenase-posttranslational facts and mysteries. *Arch. Biochem. Biophys.* **414,** 150–158 CrossRef Medline

44. Houtz, R. L., Magnani, R., Nayak, N. R., and Dirk, L. M. A. (2008) Co- and post-translational modifications in Rubisco: unanswered questions. *J. Exp. Bot.* **59,** 1635–1645 Medline

45. Lamport, D. T. A., and Northcote, D. H. (1960) Hydroxyproline in primary cell walls of higher plants. *Nature* **188,** 665–666 CrossRef

46. Cassab, G. I. (1998) Plant cell wall proteins. *Annu. Rev. Plant Physiol. Plant Mol. Biol.* **49,** 281–309 CrossRef Medline

47. Moreno, J., García-Murria, M. J., and Marín-Navarro, J. (2008) Redox modulation of Rubisco conformation and activity through its cysteine residues. *J. Exp. Bot.* **59,** 1605–1614 Medline

48. Chung, C.-C., Hwang, S.-P. L., and Chang, J. (2008) Nitric oxide as a signaling factor to upregulate the death-specific protein in a marine diatom, *Skeletonema costatum*, during blockage of electron flow in photosynthesis. *Appl. Environ. Microbiol.* **74,** 6521–6527 CrossRef Medline

ASBMB

49. Morin, B., Bubb, W. A., Davies, M. J., Dean, R. T., and Fu, S. (1998) 3-Hydroxylysine, a potential marker for studying radical-induced protein oxidation. *Chem. Res. Toxicol.* **11,** 1265–1273 CrossRef Medline

50. Smith, W. G., Gilboe, D. P., and Henderson, L. M. (1965) Incorporation of hydroxylysine into the cell wall and a cell-wall precursor in *Staphylococcus aureus. J. Bacteriol.* **89,** 136–140 Medline

51. Kröger, N., Deutzmann, R., and Sumper, M. (2001) Silica-precipitating peptides from diatoms. *J. Biol. Chem.* **276,** 26066–26070 CrossRef Medline

52. Houtz, R. L., and Mulligan, R. M. (1991) Protection of tryptic-sensitive sites in the large subunit of ribulose-1,5-bisphosphate carboxylase/oxygenase by catalysis. *Plant Physiol.* **96,** 335–339 CrossRef Medline

53. Holm-Hansen, O., Lorentzen, C. J., Holmes, R. W., and Strickland, J. D. H. (1965) Fluorometric determination of chlorophyll. *ICES J. Mar. Sci.* **30,** 3–15

54. Sargent, J. R., Eilertsen, H. C., Falk-Petersen, S., and Taasen, J. P. (1985) Carbon assimilation and lipid production in phytoplankton in northern Norwegian fjords. *Mar. Biol.* **85,** 109–116 CrossRef

55. Parry, M. A. J., Delgado, E., Vadell, J., Keys, A. J., Lawlor, D. W., and Medrano, H. (1993) Water stress and the diurnal activity of ribulose-1,5-bisphosphate carboxylase in field grown *Nicotiana tabacum* genotypes selected for survival at low $CO_2$ concentrations. *Plant Physiol. Biochem.* **31,** 113–120

56. Parry, M. A. J., Keys, A. J., and Gutteridge, S. (1989) Variation in the specificity factor of $C_3$ higher plant Rubiscos determined by the total consumption of ribulose-$P_2$. *J. Exp. Bot.* **40,** 317–320 CrossRef

57. Carmo-Silva, A. E., Keys, A. J., Andralojc, P. J., Powers, S. J., Celeste Arrabaça, M., and Parry, M. A. J. (2010) Rubisco activities, properties, and regulation in three different C4 grasses under drought. *J. Exp. Bot.* **61,** 2355–2366 CrossRef Medline

58. Yokota, A., and Canvin, D. T. (1985) Ribulose bisphosphate carboxylase/oxygenase content determined with [$^{14}$C]carboxypentitol bisphosphate in plants and algae. *Plant Physiol.* **77,** 735–739 CrossRef Medline

59. Otwinowski, Z., and Minor, W. (1997) Processing of X-ray diffraction data collected in oscillation mode. *Methods Enzymol.* **276,** 307–326 CrossRef Medline

60. Kabsch W. (2010) XDS. *Acta Crystallogr. D Biol. Crystallogr.* **66,** 125–132 CrossRef Medline

61. Vagin, A., and Teplyakov, A. (1997) MOLREP: an automated program for molecular replacement. *J. Appl. Crystallogr.* **30,** 1022–1025 CrossRef

62. Murshudov, G. N., Vagin, A. A., and Dodson, E. J. (1997) Refinement of macromolecular structures by the maximum-likelihood method. *Acta Crystallogr. D Biol. Crystallogr.* **53,** 240–255 CrossRef Medline

63. Adams, P. D., Afonine, P. V., Bunkóczi, G., Chen, V. B., Davis, I. W., Echols, N., Headd, J. J., Hung, L. W., Kapral, G. J., Grosse-Kunstleve, R. W., McCoy, A. J., Moriarty, N. W., Oeffner, R., Read, R. J., Richardson, D. C., *et al.* (2010) PHENIX: a comprehensive Python-based system for macromolecular structure solution. *Acta Crystallogr. D Biol. Crystallogr.* **66,** 213–221 CrossRef Medline

64. Winn, M. D., Isupov, M. N., and Murshudov, G. N. (2001) Use of TLS parameters to model anisotropic displacements in macromolecular refinement. *Acta Crystallogr. D Biol. Crystallogr.* **57,** 122–133 CrossRef Medline

65. Lamzin, V. S., Perrakis, A., and Wilson, K. S. (2001) The ARP/WARP suite for automated construction and refinement of protein models. In *International Tables for Crystallography, Vol. F, Crystallography of Biological Macromolecules* (Rossman, M. G., and Arnold, E., eds) pp. 720–722, Kluwer Academic Publishers, Dordrecht, Netherlands

66. Jones, T. A., Zou, J. Y., Cowan, S. W., and Kjeldgaard, M. (1991) Improved methods for building protein models in electron density maps and the location of errors in these models. *Acta Crystallogr. A* **47,** 110–119 CrossRef Medline

67. Pannu, N. S., and Read, R. J. (1996) Improved structure refinement through maximum likelihood. *Acta Crystallogr. A* **52,** 659–668 CrossRef

SASBMB

*J. Biol. Chem.* (2018) 293(34) 13033–13043 **13043**